Local and global sensitivity analysis of a coupled heat and moisture transfers model: effect of the variability of cob material properties

Junior Tchiotsop, Stéphanie Bonnet, Tristan Senga Kiessé, Nabil Issaadi, Philippe Poullain

Local and global sensitivity analysis of a coupled heat and moisture transfers model: effect of the variability of cob material properties

Junior Tchiotsop[1,2,3], Stéphanie Bonnet[1,2], Tristan Senga Kiessé[2,4], Nabil Issaadi [1,2], Philippe Poullain[1,2]

Abstract

Among earthen construction techniques, cob might be an interesting solution to mitigate greenhouse gases emissions and energy consumption of the building industry. One main issue encountered is that the cob material shows large variability of hygrothermal properties, which could consequently have an impact on the reliability of the estimation of the energy consumption of cob buildings. At the wall scale, the hygrothermal properties significantly influence the kinetics of moisture and heat transfers through the building shell, both being coupled. In order to measure the relative contribution of the variation of the hygrothermal properties, a sensitivity analysis of a coupled heat and moisture transfer model has been carried out on a cob wall. More specifically, a local sensitivity analysis has been performed (one model input wobbles around a reference value) and compared with a global sensitivity analysis, which may provide the potential interaction between model inputs. For the latter approach, the Morris method was used and allows to find the influence level of material properties and the relationships with model outputs. Two study cases have been performed: a static loading case, to find temperature and water vapour pressure profiles across the cob wall until the steady state and a dynamic loading case under a 2.5 years external dynamic loading (St-Nazaire meteorological data, France). As main results, the global approach showed in general a higher variability of properties, the sorption isotherms and the water vapour permeability were the most influential input parameters on humidity profiles while on temperature ones, the variability of both properties led up to 0.25 $°C$ variation range. The influence of thermal properties was very sensitive to the daily-loading variation while that of the hygric properties was very sensitive to the seasonal-loading variation.

Nomenclature

BCs	Boundary conditions
SI	Sorption Isotherm
SL	Static loading
SA	Sensitivity Analysis
LA	Local Analysis
DL	Dynamic loading
C_m $[kg/kg.Pa]$	Moisture storage capacity
C_p $[J/kg.K]$	Specific heat capacity
j_m $[kg/m^2.s]$	Moisture flux density
j_v $[kg/m^2.s]$	Vapour flux density
k_m $[kg/m.s.Pa]$	Moisture permeability
k_l $[kg/m.s.Pa]$	Liquid water permeability
k_0 $[m^2]$	Intrinsic permeability
k_T $[kg/m.s.K]$	Thermogradient coefficient
L_v $[J/kg]$	Evaporation latent heat
λ $[W/m.K]$	Thermal conductivity
M_w $[kg/mol]$	Water molecule molar mass
T $[K$ or $°C]$	Temperature
μ_w $[Pa.s]$	Dynamic viscosity of water
P_v $[Pa]$	Water vapour pressure
P_{vsat} $[Pa]$	Water vapour pressure at saturation
R $[J/mol.K]$	Ideal gas constant (8.314)
RH $[\%]$	Relative humidity
ρ_w $[kg/m^3]$	Water density
ρ_s $[kg/m^3]$	Material apparent density
σ_0 $[-]$	Phase change coefficient
$w[kg/kg]$	Water content
T_{int} $[K$ or $°C]$, RH_{int} $[\%]$	Interior Temperature and RH
T_{init} $[K$ or $°C]$, RH_{init} $[\%]$	Set point temperature and RH

✉ Stéphanie Bonnet
stephanie.bonnet@univ-nantes.fr

[1] Nantes université, GeM UMR 6183, F-44600 Saint-Nazaire, France

[2] IRSTV, CNRS FR2488, Ecole Centrale de Nantes, 44300 Nantes, France

[3] Agence de l'environnement et de la Maîtrise de l'Energie 20, avenue du Grésillé- BP 90406, 49004 Cedex 01 Angers, France

[4] INRAE, Institut Agro, SAS, Rennes, France

1 Introduction

The French "Grenelle 1" act of 2009 considers transportation and construction as the most decisive action-levers for a fourfold reduction in the carbon balance by the year 2050. According to the French Environment and Energy Management Agency (ADEME), the share of heating in the total energy consumption of buildings is approximately 61% for residential buildings and 49% for tertiary buildings and all represent 19% of greenhouse gases emissions [1]. One engineering challenge remains to accurately estimate the needs in energy, to ensure occupants comfort. This can be done either during the design step of new buildings to get more energy-efficient buildings or through energy retrofitting of the existing buildings using efficient insulation materials, i.e., materials adapted to the wall composition and taking into account the characteristics of the old building materials [2, 3].

Thus, earthen constructions appear to be an eco-friendly solution. They have a low embodied energy and good hygrothermal properties, to provide indoor comfortable environment [4, 5]. Moreover, they are built using low-technology construction techniques, do not require any heavy processing and can be reused easily after deconstruction [5]. Despite all these advantages, there is still a need for improving the characterization protocols of the hygrothermal properties for earthen composites, especially cob materials properties, which may vary considerably from one composite and local architecture to another [5]. Therefore, it becomes difficult to establish clear recommendations on the various properties of the material to assist engineers during the design stage [5].

One of the main issues raised by using earth in constructions is the accurate modelling of heat and moisture transfers through walls responding to temperature and relative humidity changes. A survey of the literature reveals that a considerable amount of efforts has been devoted to the development of coupled models [6–10]. These models are phenomenological-based on various assumptions at the micro-structure scale. Unlike heat transfer models, including three inputs (heat capacity, density and thermal conductivity), coupled heat and moisture transfer models have at least seven (heat and moisture coupled transfer) [8, 9] or ten (heat, moisture and air transfers) inputs (for two or three driving potentials, respectively) [7, 10]. Hence, a model is chosen according to compatibility among driving potentials, building structure and material properties. Unfortunately, numerous model inputs are usually related material properties and could not be always determined by conventional experimental protocols, and if so, may be subjected to non-negligible measurement variability. For instance, the variation of cob material properties could be due to:

- the local source of the material, usually in a close environment to the construction site like in Brittany and Occitania (France) [11–13],
- the construction technique, that is related to the vernacular architecture [14, 15],
- the use of admixtures or binders [16–20],
- the use of plant fibres [21–25],
- the measurement techniques [26],
- the uncertainties of the technical ability and skill of the operator during construction or material characteristic assessment stages.

Baescher and Christian [27] ranged the variabilities into three main groups: 1) the knowledge uncertainty - 2) the decision model uncertainty, on which human decisions can influence and thus can be reduced/annihilate - 3) the natural variability which cannot be handled. The present work focuses on the latter variability, as being an intrinsic characteristic to describe the cob material.

The Sensitivity Analysis (SA) is a statistical approach used to examine how a model inputs' variability influences the model outputs. For instance, SA aims to: (i) rank model inputs according to their influence level on outputs, (ii) identify non-influential inputs for model reduction, (iii) calibrate input range using inverse analysis of actual output data (experimental) [28, 29]. In the building domain, the SA is usually carried out at the building scale to validate insulation design for energy-efficient housing (energy consumption) and to determine the influential characteristics [30–33], the assessment of the environmental impacts [30, 34] and the sustainability of structures [35, 36].

To assess the influence of the material properties scarcity got from experimental characterization on coupled heat and moisture transfers, many authors generally perform a local SA (also called parametric study), which consists in the valuation of the model response by varying each input around a reference value, like the mean value for instance.

Following this approach, Othmen et al. [37] have assessed the effects of the variations of limestone material properties (±5%) and heat convection coefficient (±10%) on Kunzel's coupled hygrothermal transfer model. They have found a relative error of 2-5% depending on the model's input. In addition, Le Tran et al. [38] have shown that combined effects may reduce output error range. They have provided details on hemp concrete characteristics (water content-dependency of properties) and the effect of ventilation on a transient hygrothermal transfer process. They have also demonstrated that even a 50% change in the thermo-diffusion coefficient did not affect moisture migration.

As an alternative to the local SA approach, the global SA is used to investigate the variations of model outputs

by varying inputs over the whole hyperspace of inputs, such that the potential interactions among inputs could be discovered. For instance, the RBD-FAST method (developed in [31]) was used as a global SA approach to determine the influence of rammed earth materials on the vapour pressure outputs of a coupled model, under a dynamic load over one year time modelling [39]. They have shown that the sorption curves broadly provide about 80% of the variance on vapour pressure outputs. Issaadi [40] has established a correlation between 4 hygrothermal inputs of concrete(moisture diffusivity, density, specific heat capacity and thermal conductivity) through a fractional factorial design method, that is a weaker version of the global sampling. He has found a relative error up to 64% on Relative Humidity (RH) outputs.

As outcome, the variability of transfers are function of the material, the variation ranges of material properties and the potential interactions among the latter. Physically, they are strongly related to the material micro-structure and behaviour. This makes the choice of the global SA approach as being suitable for performing SA of a coupled heat and moisture transfers model in comparison with the local SA approach. In this way, this paper presents the results of the SA conducted on a coupled heat and moisture transfers model for cob materials using both local approach and the Morris method [41] as a global approach. The main objectives are to find:

- the influence level of cob material properties variation ranges on a coupled hygrothermal model outputs by using the Local Analysis (LA) and the Morris Method (MM) in order to potentially reduce the model.
- the significance of cob properties' influences during seasons
- the existing relationship between cob properties and the model outputs.

2 Materials and methods

2.1 Hygrothermal transfer model

The model used herein has been written by the Laboratory of Engineering Sciences for the Environment (LaSIE) of la Rochelle University. It has been validated for various bio-based and earthen materials [7, 42–44]. As model assumptions, the cob material is assumed to be a porous medium with earthen grains as rigid solid phase, a pure capillary water as liquid phase and water vapour as gaseous phase (assumed to be an ideal gas). Radiation and convective heat transfer inside the material are neglected in comparison to conduction. Temperature (T) is used as heat driving potential while the water vapour pressure (P_v) is the moisture driving potential. The transport of liquids at the level of the capillary pores and the transport of water vapour are described by Darcy's law and Fick's law, respectively. The sensible heat flux follows Fourier's conduction law and the latent heat of evaporation/condensation is considered in the water phase change. The following coupled hygrothermal transfer model is obtained from the combination between the heat and moisture balance equations and the Kelvin-Laplace equation (assuming a local thermodynamic equilibrium between material phases):

$$\begin{cases} \rho.C_m.\frac{\partial P_v}{\partial t} = \vec{\nabla}\cdot\left(k_m.\vec{\nabla}P_v + k_T\vec{\nabla}T\right) \\ \rho.C_p.\frac{\partial T}{\partial t} = \vec{\nabla}\cdot\left(\alpha\vec{\nabla}P_v + \lambda.\vec{\nabla}T\right) + L_v.\rho.C_m.\sigma_0.\frac{\partial P_v}{\partial t} \end{cases} \quad (1)$$

The variables are described in the Table 1:

This model proves adequate for earthen materials because only two properties (k_T and σ_0) are difficult to be measured and the other inputs are material properties measured in

Table 1 Model inputs description

$C_m = \frac{1}{P_{vsat}}.\frac{\partial w}{\partial RH}$	$k_m = k_v + k_l^*$	$\sigma_0 = \frac{div\left(\vec{j_v}\right)}{div\left(\vec{j_m}\right)}$	$\alpha = h_l.k_m$
$k_l = \frac{k_0.\rho_w}{\mu_w}$	$P_v = RH.P_{vsat}(T)$	$k_l^* = k_l\left(\frac{RT\rho_w}{M_w}.\frac{1}{P_v}\right)$	
$P_{vsat}(T) = 23.5771 - \frac{4042.9}{T-37.58}$		$k_T = -k_l\left[\frac{RT\rho_w}{M_w}.\frac{\partial ln\left(\frac{P_v}{P_{vsat}}\right)}{\partial T} + \frac{R\rho_w}{M_w}.ln\left(\frac{P_v}{P_{vsat}}\right)\right]$	

k_l $[kg/(m.s.Pa)]$	liquid water conductivity	k_0 $[m^2]$	intrinsic permeability
ρ_w $[kg/m^3]$	liquid water density	$\mu_w(T)$ $[Pa.s]$	dynamic viscosity of water
$R = 8.3145$ $[J/(mol.kg)]$	ideal gas constant	M_w $[kg/mol]$	Water molar mass
P_{vsat} $[Pa]$	water vapour pressure at saturation	w $[kg/kg]$	water content inside the material
RH $[\%]$	Relative Humidity	h_l $[J/kg]$	Enthalpy of the liquid water
L_v $[J/kg]$	Evaporation latent heat		

laboratory at material scale. Also, inputs are material properties and they can be directly measured without needing intermediate models. Hence, as model inputs, there are:

- the dry bulk density (ρ [kg/m^3])
- the hygric capacity (C_m [$kg/(kg.Pa)$]) which is a function of the slope of the Sorption Isotherms (SI) of the material
- the moisture permeability (k_m [$kg/(m.s.Pa)$])
- the specific heat capacity (C_p [$J/(kg.K)$])
- the thermal conductivity (λ [$W/(m.K)$]).
- the coupling inputs: k_T [$kg/(m.s.K)$] that represents the liquid infiltration under a temperature gradient and σ_0 [$-$] which is the phase-change coefficient of the cob material. The latter is the ratio between the divergences of water vapour and moisture fluxes – the moisture flux is assumed as being the sum of the water vapour and the pure liquid water fluxes.

2.2 Characterization of the model inputs

The variation range of hygrothermal properties (ρ_s, k_m, λ, C_p and SI) of the unfibred cob material were collected from the literature [13, 24, 26, 45–50]. We proposed to find the effect of the reproducibility of materials properties. Indeed, the variabilities include the natural variability, the inter-laboratory, the fabrication protocol, the test protocols and the soil texture variabilities. The variation ranges of the unfibred cob material properties are reported in Table 2. However, the significant discrepancy observed between data, cannot be attributed to natural variability given the small number of repetitions of the tests (3 - 12).

Data for the liquid permeability (k_l) and the intrinsic water vapour permeability (k_0) of adobe/cob material are lacking because of the measurement difficulty for earthen material without binder, due to their friable behaviour. However, Janssen [51], Fabbri et al. [52, 53] have assessed (k_0), using oedometer and using correlation with water absorption (model + measurements) for rammed earth. They found a negative correlation with the dry bulk density for rammed earth materials and values ranging from $1.0 \times 10^{-17} m^2$ ($2.2 g/cm^3$) to $4.0 \times 10^{-17} m^2$ ($1.7 g/cm^3$). Because soil compaction reduces the porosity and increases the material tortuosity [54, 55], the liquid permeability of cob material (lower compaction but with high clay content) is assumed to be higher than rammed earth one.

For convenience in this analysis, the infiltration coefficient k_T was assumed to be constant to ($1.0 \times 10^{-6} kg/m.s.K$) as well as the phase-change coefficient σ_0 (0.8). As matter of fact, there is no literature data related to the coupling inputs on earthen materials. Moreover, Tchiotsop [56] has found through a numerical analysis of k_T expression that it fills a high range variation for cob material (10.10^{-10}–5.10^{-6} kg/m.s.K). The higher are T and P_v, the higher is k_T. Hence, we assumed for the analysis that the water vapour transfer is mostly carried out by the thermo-diffusion effect. Concerning the phase-change coefficient σ_0, a parametric analysis has shown that σ has a low influence on driving potentials [56]. Varying σ_0 from 0 to 1 has led to negligible variation of 0.20 deg C on T and $40 Pa$ on P_v.

In the model, the moisture storage (C_m) is related to the slope of sorption isotherms (SIs). As hysteresis between adsorption and desorption curves are low for unfibred earthen materials [26, 57], it was assumed to be negligible. Same for the temperature-dependency of sorption isotherms. The data collected are measured using Saturated Salt Solutions (SSS) and Dynamic Vapour Sorption (DVS) methods (Fig. 1a). The water content at each RH of the latter were regularly-meshed between the lower and upper limits despite the great correlation between corresponding water contents. The found curves were fitted using a GAB model to be used as input for Morris algorithm (Fig. 1b) [58].

Because the present study focuses on the contributions of the material properties, other sources of variability such as the wall thickness, the indoor occupancy and the weather were not considered. Indeed, as found by Goffart [59] and Tzuc et al. [60], the effects of regional environment variability can reach up to 90% of the variability of the energy needs estimation of a building. For so, the study focuses on the evolution trends with external loading evolution. The indoor ambience is kept stable.

The simulations were conducted for a 300 mm thickness cob wall (Fig. 2). the wall lower and upper faces are assumed to be perfectly insulated and water-tight (moisture and vapour). The set-point conditions of the wall were

Table 2 Variation ranges of the material properties and reference data

Input	References	Range	Reference data
$\rho_s[kg/m^3]$	[13, 24, 26, 45–50]	1700 - 2000	1850
$k_m[kg/m.s.Pa]$	[13, 26, 48]	1.0×10^{-11} - 7.0×10^{-11}	3.5×10^{-11}
$\lambda[W/m.K]$	[13, 26, 45–47, 49]	0.4 - 1.2	0.9
$C_p[J/kg.K]$	[13, 24, 26, 46, 47, 49, 50]	790 - 950	850
$\sigma_0[-]$	-	0.8	0.8
$k_T[kg/m.s.K]$	-	1.0×10^{-6}	1×10^{-6}

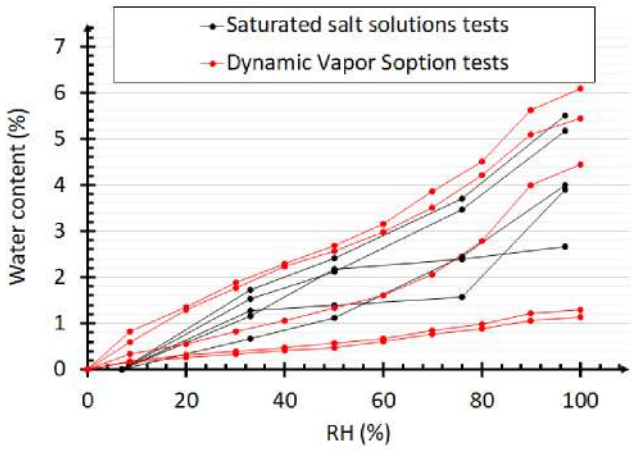

(a) Experimental curves [26, 50]

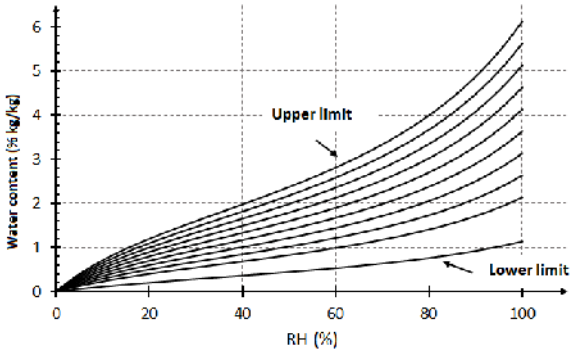

(b) GAB model results of meshed isotherms

Fig. 1 Meshed sorption isotherms (SIs)

assumed to be the initial conditions of the outer dynamic loading, as 8.1 °C for T and 86% for RH ($P_v = 930\ Pa$). The inner conditions were kept constant (20 °C and 60% for RH corresponding to a P_v of 1404 Pa). Regarding the outdoor weather conditions, a Static Loading (SL) condition of 10 °C and 80%RH ($P_v = 983\ Pa$) was firstly applied. Next, the Montoir-station climatic data of Saint-Nazaire (France) were provided for a Dynamic Loading (DL) case (Fig. 3). It represents data from the 1st January 2019 to the 31st August 2021. Dirichlet boundary conditions were assumed for heat and moisture transfers to discard the effect of the uncertainties of the heat transfer coefficient, which is not the aim of the present study.

Calculations were performed using the COMSOL Multiphysics PDE solver and its Matlab Livelink module to perform Morris method algorithm (Fig. 4). The simulations were carried out with a time-step of 2 h during two months for the SL case and during 973 days for DL. The time period of 973 days for the DL was previously found to be the shortest period allowing to study the wall response by discarding the effect of the initial conditions of the wall, especially for the moisture transfer. Of course, as found by Bui et al. [39], a rammed earth wall reaches after one year some kind of steady behaviour with seasonal variations independent on the initial condition, as well for heat transfer as for moisture transfer.

2.3 Sensitivity analysis methods

2.3.1 Morris method

The model written in Eq. (1) can be represented as a connecting function of an outputs vector y with inputs vector $x = (x_1, x_2 \dots x_k)$ with k coordinates, assumed to be independent. Each input x_i is normalized and meshed in p regular

Fig. 2 Wall geometry and boundary conditions

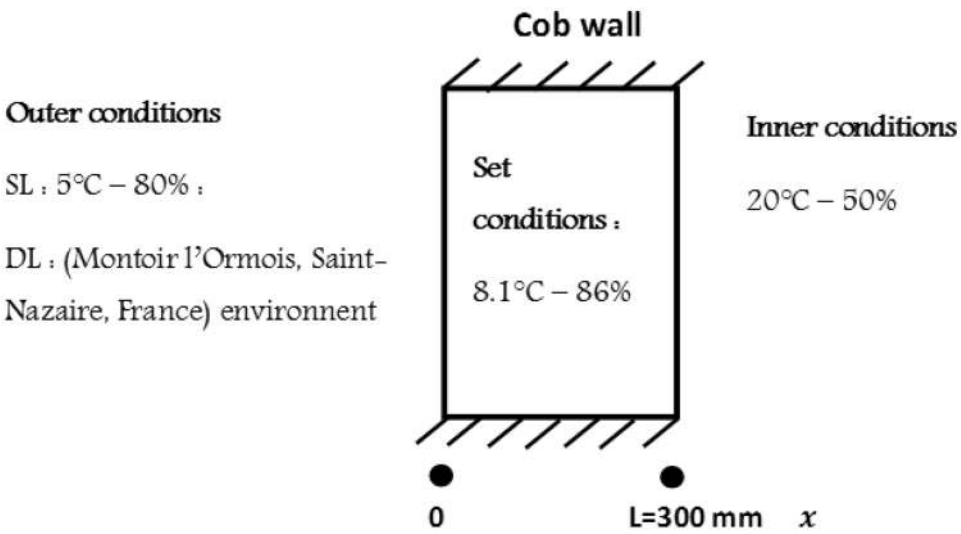

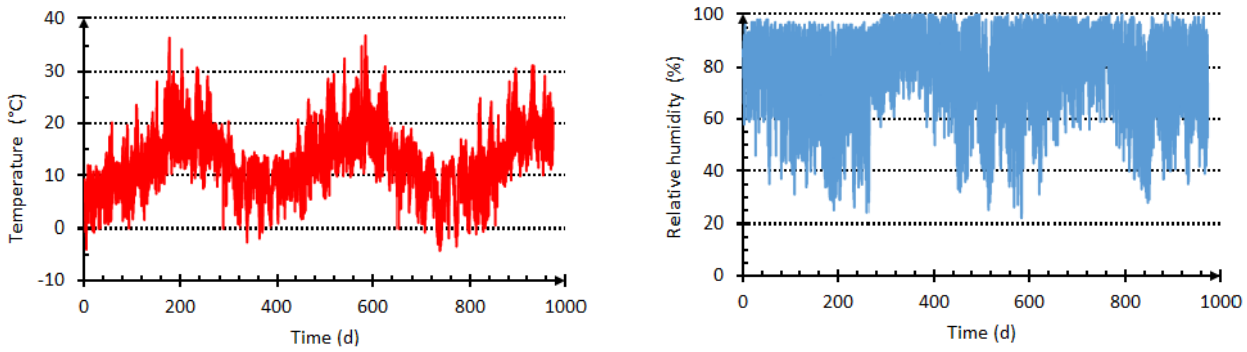

(a) Temperature

(b) Relative humidity

Fig. 3 Montoir l'Ormois station climatic data from 1^{st} January 2019 to the 31^{st} August 2021 (Saint-Nazaire, France)

steps within its variation range. A sequence of $k+1$ points $x^{(0)}, x^{(1)} \dots x^{(k)}$ is randomly simulated so that two successive points differ by one coordinate, e.g. $x^{(0)} = (x_1, \dots, x_j, \dots, x_k)$ and $x^{(1)} = (x_1, \dots, x_j \pm \Delta_x j, \dots, x_k)$ with Δx_j a fixed step for each input x_j. This means that only one input varies between two successive points of a sequence (one-at-a-time method). The sequence of $k+1$ points makes it possible to compute the so called "elementary effect" ee_i of the i^{th} property obtained by the difference between the model evaluations at two successive points, namely:

$$ee_i = \frac{f(x_1, x_2, \cdots, x_i + \Delta x_i, \cdots, x_n) - f(x_1, x_2, \cdots, x_i, \cdots, x_n)}{\Delta x_i}. \tag{2}$$

A number r of random sequences of $k+1$ points are generated and the following indices are computed for each input x_i:

- the mean of elementary effects $\mu_i = \frac{1}{r}\sum_{i=1}^{r}(ee_i^k)$,
- the standard deviation (σ_i).

In order to get an unbiased effect of inputs, the mean of absolute values of elementary effects $\mu_i^* = \frac{1}{r}\sum_{k=1}^{r}|ee_i^k|$ is computed (see Morris [41] for more details). Meshing of sorption isotherms was carried out uniformly for each *RH* loading water contents, between the highest and lower ones (Fig. 1b) in order to adapt adsorption curves for the Morris method. All adsorption curves were fitted using a GAB model [58] and GAB model parameters groups were used as meshing input during sampling step.

For better understanding of the input influence, the following rules were stated [30]:

- The higher the μ^* of an input is, the higher the influence on the output is.
- $\sigma/\mu^* \leq 0.1$ indicates a linear relationship between inputs and outputs.
- $0.1 < \sigma/\mu^* \leq 0.5$ indicates a monotonic relationship between inputs and outputs.
- $\sigma/\mu^* > 0.5$ indicates a non-linear relationship between inputs and outputs and/or an interaction between inputs.

Moreover, the sign (positive or negative) of μ_i indicates the sense of the effects of an input on the output, for instance, $\mu_i > 0$ suggests a positive correlation with the model output, and vice versa.

The following values for the Morris method were considered: $p = 10$ for the discretization levels with a fixed step $\Delta = 0.56$ and $r = 30$ repetitions of the sequence, which gives $r(k+1) = 240$ model evaluations with $k = 7$ model inputs.

The influence of inputs on outputs was also examined using local analysis (LA) after data were divided using five values within their variation range, for comparison with the Morris method results.

Figure 4 describes the computation algorithm with Morris method:

However, the Morris method itself does not always provide repeatable quantitative sensitivity indices to measure the contribution of the model inputs variability of outputs' ones. It provides only a preview of the parameters' influence level as well as a classification for model reduction. That is relative to the randomized sampling, especially the numbers of levels (repetitions), the meshing of the hyperspace, the inputs distribution, etc.

2.3.2 Descriptive statistic tools

The coefficient of variation of the outputs with respect to inputs variation are used to assess the uncertainty obtained from the local analysis (LA) and the Morris method (MM).

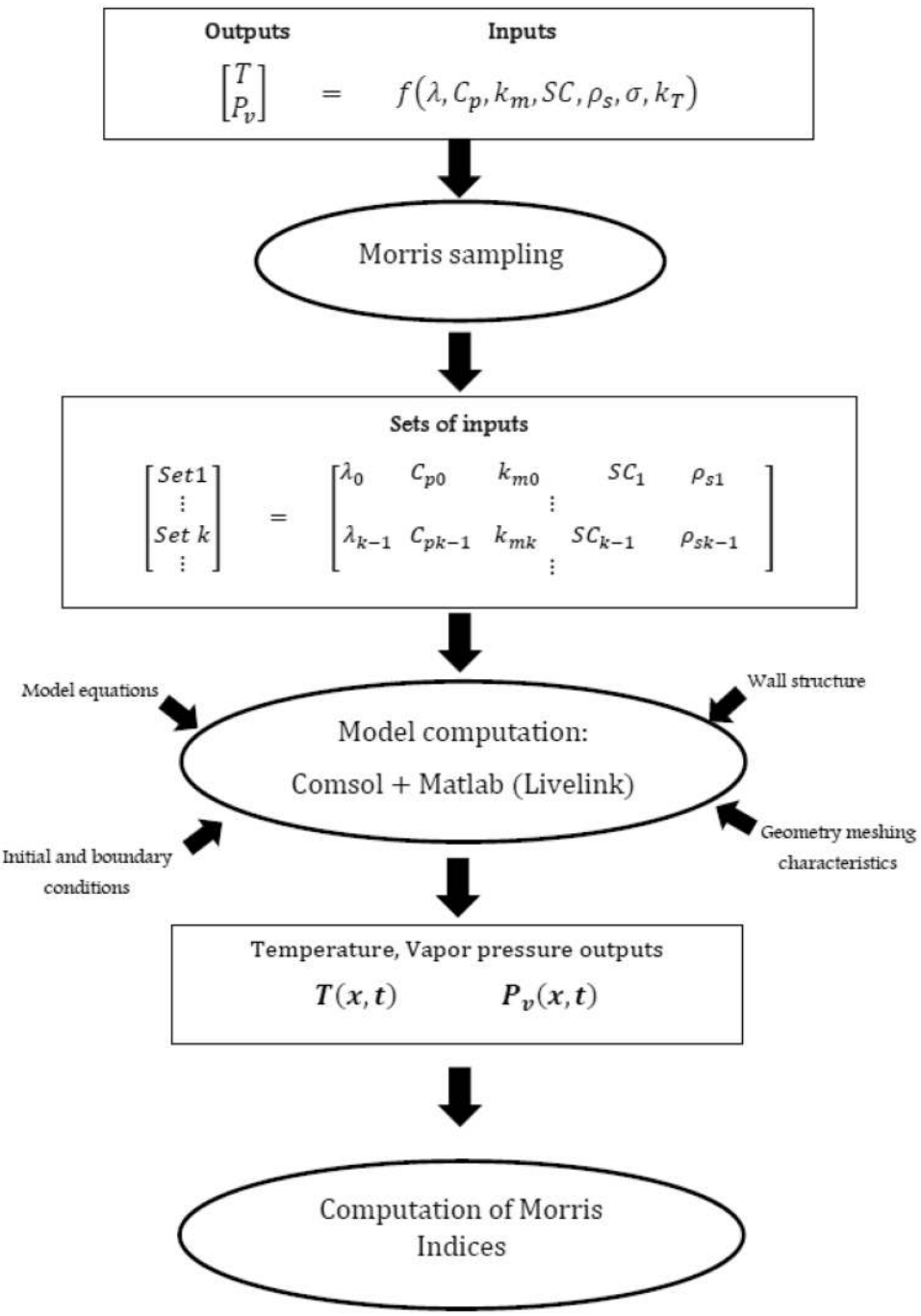

Fig. 4 Morris sensitivity analysis algorithm applied to the chosen HT transfer model

The 5th and the 95th percentiles were also used to rank the relationship between inputs and outputs as they were continuous series (over time). The lower is the 95th percentile, the more linear is the relationship between the considered input and output. Moreover, we used the difference between the two latter percentiles of σ_i/μ_i^* ratio (named as θ_i) as the noise indicator of each input with respect to each output. The higher is θ_i, the noisier is the input with respect to the output and therefore, the probability of the property to be interactive is high.

Finally histograms of model results were plotted in order to analyse the decay between deterministic (handled by the basis set of inputs), the LA and the MM approaches.

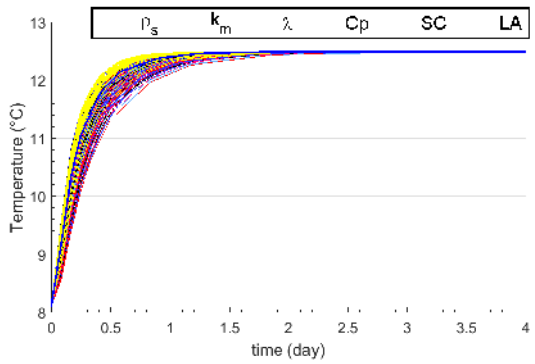

(a) Static loading: profiles of T at wall mid-depth (GA and LA)

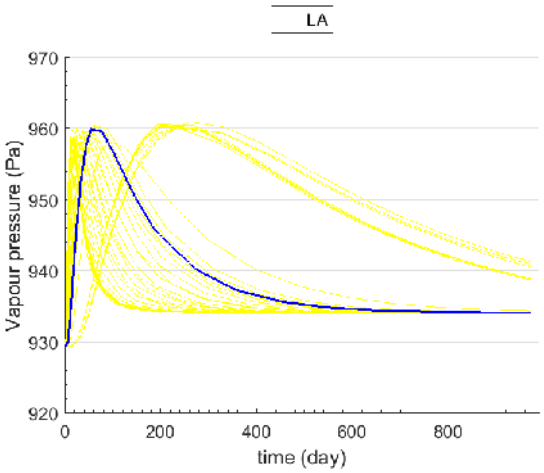

(b) Static loading: profiles of P_v at wall mid-depth (LA)

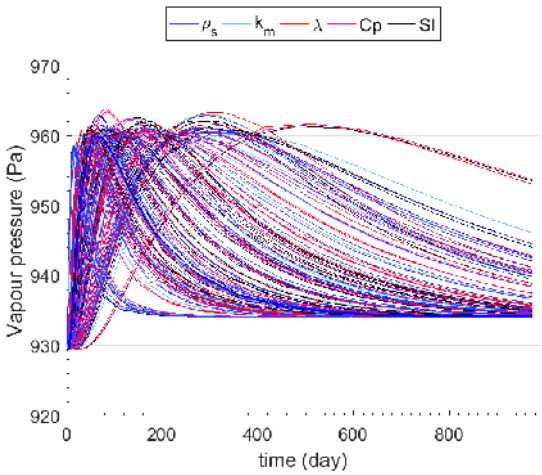

(c) Static loading: profiles of P_v at wall mid-depth (GA)

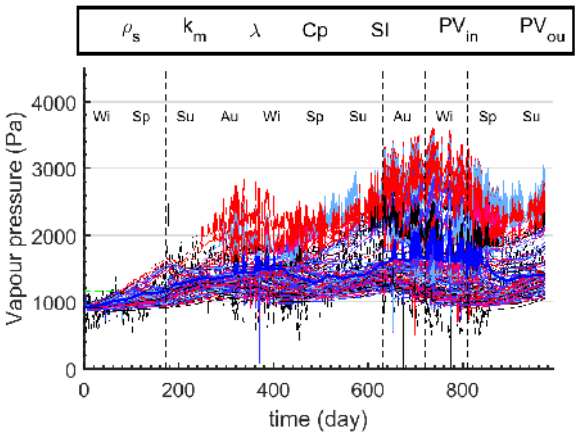

(d) Dynamic loading: profiles of P_v at wall mid-depth (GA)

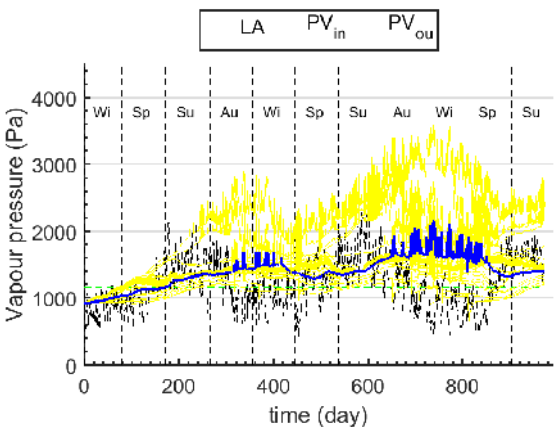

(e) Dynamic loading: profiles of P_v at wall mid-depth (LA)

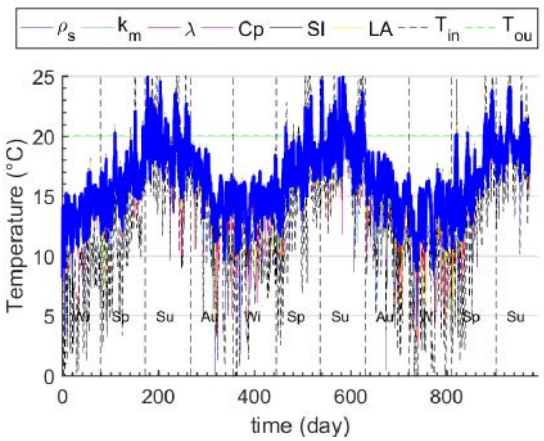

(f) Dynamic loading: profiles of T at wall mid-depth (GA and LA)

◂**Fig. 5** Wall responses. Yellow curves are the wall responses beam to properties variation using LA (55 input data sets) and coloured curves using MM (180 inputs data sets). Blue-weighted curves are the responses corresponding to the basis set of input

3 Results and discussions

3.1 Effects on transfer kinetics

3.1.1 Static loading case

Figure 5a and c display the variability of temperature and water vapour profiles, for the static loading case, at the mid-depth of the wall. The Local Approach (LA) results is represented by yellow curves and Morris method (MM) ones by the other coloured curves. The mid-depth have been chosen as it undergoes the effects of outer and inner loadings in a balanced manner. The mid-depth is highly dependent on the gap between outer and inner loadings, as shown on Fig. 7a–d, highlighting the profiles variability according to the wall depth.

The transient stage of the static loading cases showed that the speed of transfer (time to the steady state) of the cob wall response is lower for heat than moisture transfer, for any set of input data. It was found to be approximately 10-12 times higher: Philip and De Vries have estimated the ratio to be around 8 [8]. In addition, the Morris method (MM) showed that some particular sets of inputs tend to slow down the transfer kinetic inside the cob wall. Indeed, the wall did not reach a perfect equilibrium until 973 days.

A higher variability on both driving potentials was found during transient phases and a quite null variation of profiles at steady states. In regards to the sampling approach, Morris method showed an increasing moisture buffering activity inside the wall, leading to a steady state time around 700 days instead of 365 for Local analysis of inputs.

3.1.2 Dynamic loading

Figure 5f and e display the temperature and the water vapour pressure profiles, respectively, computed at the wall mid-depth (150 mm) for the Dynamic Loading (DL) case.

Profiles show a transient phase during the first year, during which the water vapour pressure strongly evolves from the set point conditions (1000Pa) to a higher value (up to 2500Pa). After 1 year, there was a global fluctuation of profiles whatever the cob wall depth, sign of an equilibrium state of moisture transfer inside the material (No more effect of set point conditions). There was a positive and variable time gap according to the set of inputs. Indeed, the first loading peak of water vapour pressure was observed around the day 200 while at 50 mm depth, it was found around the day 300 and up to the day 360 at 100 mm position (Fig. 13). These results were more reliable as no hysteresis on sorption isotherms is assumed. Indeed, a higher hysteresis could reduce the time decay, because the residual moisture inside the wall increases at the end of each daily moisture desorption. Most of profiles were not sensitive to the outer daily P_v loading variability, for both local and global approaches. Taking into consideration the time decay, profiles were always slightly lower than the corresponding water vapour saturation during a long period (Fig. 13). From that moment, a quite steady adsorption and desorption slopes with respect to time were found. Approximately the same time of transfer equilibrium state is found for rammed earth [39].

P_v profiles showed a large gap of profiles unlike T profiles. The latter profiles were hidden by the basis set of inputs response (blue-weighed curve). Moreover, there was a decreasing variability during desorption phases (days 300–440 for instance) in contrast to adsorption phases (day 440–600 for instance). Unlike the water vapour profiles, there was a negligible variability of temperature profiles. The latter was very sensitive to the external loading variability: as far as the depth is closer to the inner side of the wall, temperature profiles daily-fluctuation decreased.

The Fig. 6 displays the variation ranges (CV) of the model outputs (T and P_v) at the mid-depth of the wall at the day 680, using the Local Analysis (LA) and the Morris Method (MM). That day was chosen as the variability of P_v profiles is close to the highest one. The Morris sampling significantly increased the variability of P_v profiles. A quite null CV was found with LA for both models inputs on P_v output, except for hygric properties. Coefficient of variations (CVs) of 16%, 33% and 28% were found due to the variability of ρ, λ and C_p inputs, respectively. Whilst, k_m and SI values showed quite the same CV for both approaches. Indeed, CVs of 30-31% and 28-26% were found using MM-LA sampling. These results seemed to be logical as for the global sampling, even the hygric properties changes when varying thermal inputs. Thus, the real effect of inputs will be found using Morris indices computation (Section 3.2). This gap in variation between the two approaches for P_v model output was found for 4 seasons in the mid-depth of the wall and showed variability of profiles always under 40% (Figs. 14 and 15).

In winter, spring and autumn seasons, when there is negligible gap of P_v loading, the effect was found quite symmetrical with a middle close to 150 mm depth whilst in summer, a P_v gap of about 1700 Pa shifted the maximum effect (and variability) near the outer wall surface. LA and GA curves highlight the high moisture buffering in earthen materials and showed that a local analysis could be sufficient to describe the variability of model responses. Moreover, Fig. 7e and f display the distribution of the P_v response at day 680 in the wall mid-depth for LA and MM respectively. It also describes with a blue line the P_v response for the reference set of model inputs. The latter displays also that a

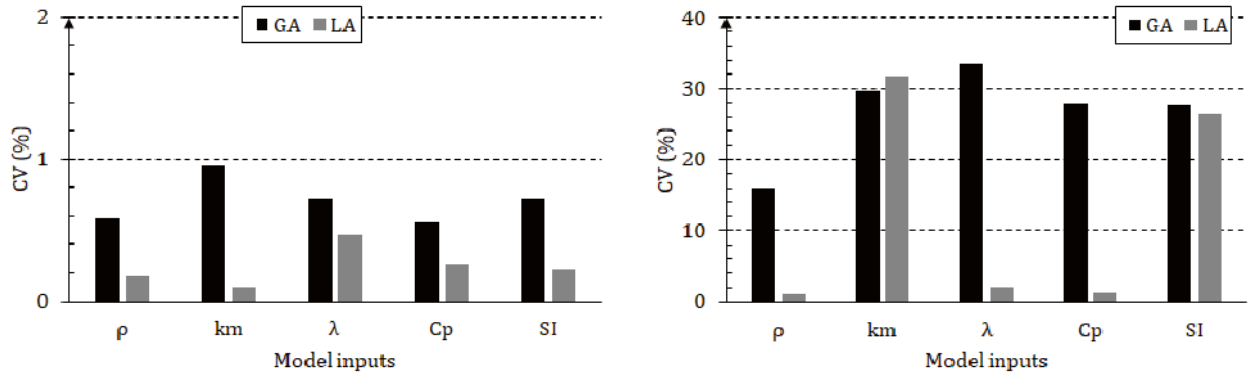

(a) Temperature (T)

(b) Water vapour pressure (P_v)

Fig. 6 Coefficient of variation of profiles at the wall mid-depth, hour 680

deterministic simulation leads to a closer P_v mean response than modal response, for the unfibred cob wall.

The variability on temperature profiles was found to be negligible, except for the thermal conductivity, for which the influences were quite the same whatever the method. That means the latter property is responsible for the minor differences between the transfer profiles displayed in Fig. 5a. On T output, a CV lower than 2% was always found for each model input and whatever the sampling approach. For MM, CVs were slightly higher for each property: there could be either a sampling effect as P_v and/or a potential interaction between properties that will be handled by θ -index of Morris algorithm.

3.2 Influence of inputs using Morris indexes

As a reminder, the μ^*-index of an input represents the mean variability of the model's outputs due to the inputs variability with numerous sets of co-input values. Figure 8a and b display the unbiased effects (μ^*) of the material properties on P_v and T outputs, at the mid-depth of the wall with respect to time. On P_v, until one year, the effects increases quite linearly until a moment when profiles are noisy. The corresponding time increased as closer as the depth is to the inner surface of the wall – it was found up to 2 years at 200 mm depth. It corresponds also to an equilibrium state of moisture transfer, as the wall is at an equilibrium state of transfers and there is no more effect of initial set conditions of the wall. The noisy effect means the material moisture is close to saturation and the liquid water transfer becomes predominant.

The sorption isotherm (SI) was the most influential input, with a μ^*, up to 1500 Pa. A value up to 2000 Pa was achieved, according to the wall depth (Fig. 13). The gap with other material properties effects increased with time. Next comes the water vapour permeability (k_m), showing a μ^* up to 1000 Pa, whereas the other inputs effects exhibited comparable values on the wall behaviour (up to 200 Pa). As global trend at the equilibrium state of transfer, μ^* for every model inputs increased from the beginning of the summer to the end of winter. The moisture migration time gap is therefore found,as the outer loading increase from the winter to summer. A seasonal influence on the effect of the SI appears clearly from these calculations.

A daily-fluctuation of the effects was found, related to the climatic loading and substantiated by the profiles through the thickness. SI showed therefore highest amplitudes around 1000 Pa, mostly visible during autumn, winter and partially during spring seasons. At 50 mm position (Fig. 13), the wall has undergone the effect of the outer loading and thus, showed a fluctuation of effects slightly higher than the loading one. This increased up to 100 – 150 mm and then decreased due to static inner loading. The increasing fluctuation effect is related to the time gap of transfers.

The Fig. 9 ranks the influence of material properties on P_v output, through the wall depth. The rank was clearly identified: the SI was the most influential model input, next came successively k_m, λ, C_p and ρ. Near walls boundaries (0–0.1L and 0.9L–L), some misclassification of the effects were found, mostly at outer face. This is explained by the non-smoothness of the loading assumption. Indeed, an obvious null effect was found at boundaries because of the prescribed Dirichlet boundary conditions. In addition, the wall inertia was not sufficient to counteract the outer loading.

The effect on the temperature output (T) were negligible (Fig. 10). As the wall was sensitive to the thermal response, the values of the effect rapidly reach a representative μ^* index. No seasonal effect was observed unlike for the moisture transfer. This could be interpreted as each input has the same influential level on T output, around 0.25 °C by mean. However, a slightly decreasing effect of inputs was noticed during autumn and winter seasons.

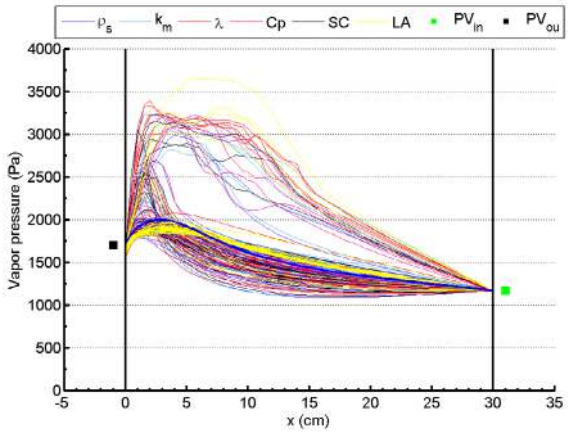

(a) day 600: summer

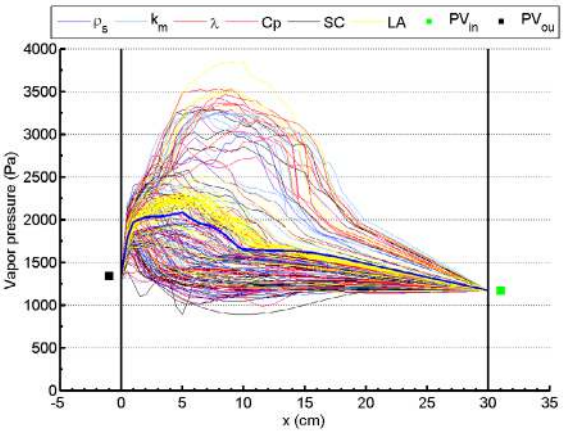

(b) day 680: Autumn

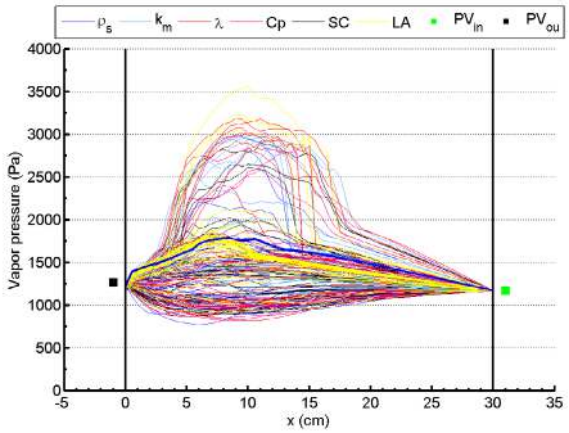

(c) day 760: Winter

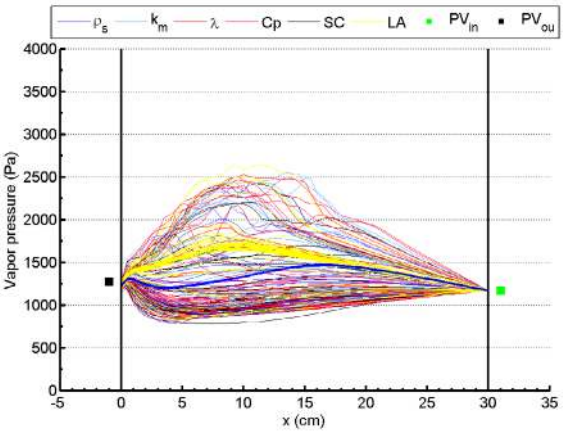

(d) day 860: Spring

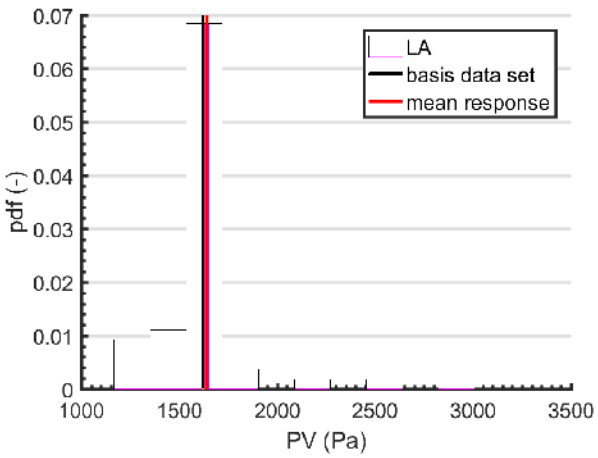

(e) PDF, LA, day 680, Spring

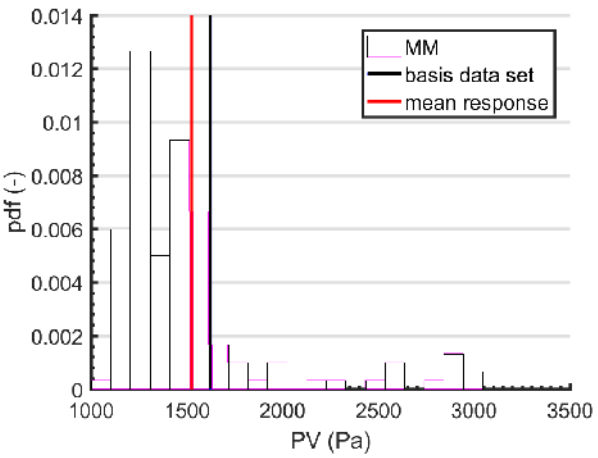

(f) PDF, MM, day 680, Spring

Fig. 7 Transversal profiles. Blue-weighted curves are the responses corresponding to the basis set of inputs

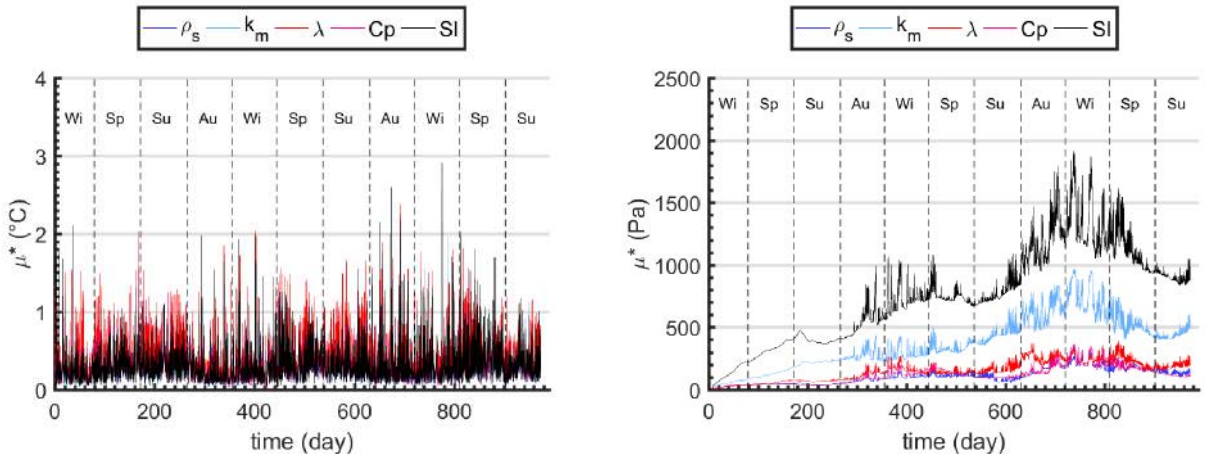

(a) On T output (b) On P_v output

Fig. 8 μ^* indices of inputs with respect to time at 150 mm position (mid-depth), for P_v and T outputs

Observed peaks occurred when significant change in temperature gradient loading was found (near days 160 and 780 for instance). As P_v profiles, a linear decrease of μ^* was found through the wall thickness for each parameter. Once again, the closer to the outer surface the depth was, the higher was the influence of the parameters on the wall response as well as their variability (noise). No clear influential classification was established. Thus, the wall response was sensitive to both the material properties and the dynamic conditions applied at the outer boundary which was already emphasized by the seasonal variations of the effects on the vapour pressure.

The Fig. 11 displays the evolution of the μ-index of inputs with respect to time t (in day), for both model inputs and outputs, at the mid-depth of the cob wall. As one could expect, given the values of μ^*, the effects of properties variation on temperature output were found centred to the null value, and depends on the seasonal variations. Indeed, the effects variability (noise) were greater during spring and summer and lower in autumn and winter. A high noise was found for SI, λ and C_p properties.

SI and k_m showed negative values of μ, with a seasonal amplitude effect. That means the higher were these properties, the lower was the P_v. This matches with the physical phenomenon of moisture transfers. Indeed, a higher k_m means a high pore connectivity and a lack of capillary suction whereas a high moisture adsorption (SI) means a high formation of bound water, for instance. Thermal properties (ρ and C_p) showed a low positive effect on P_v output. The material density ρ showed a fluctuating negligible effect

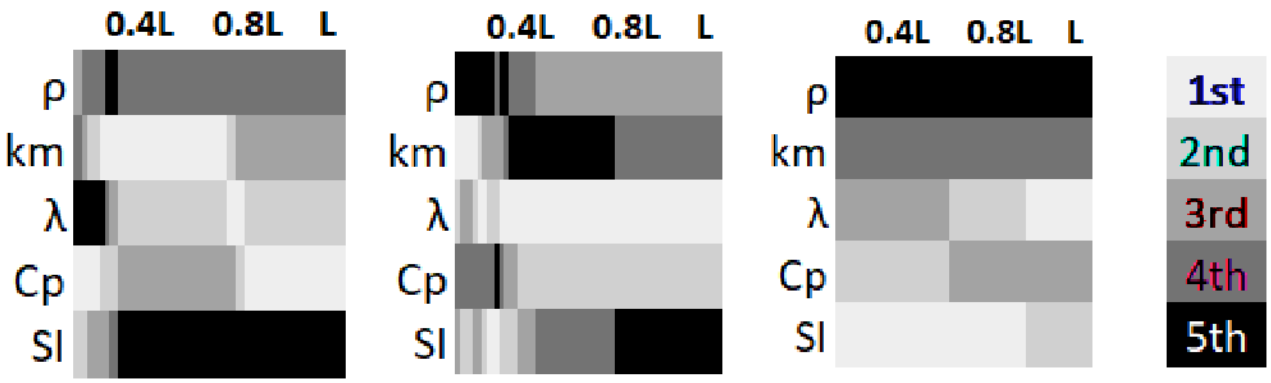

(a) Day 600 (summer) (b) Day 680 (autumn) (c) Day 760 (winter)

Fig. 9 Ranking of the influence of material properties through the wall depth for P_v output

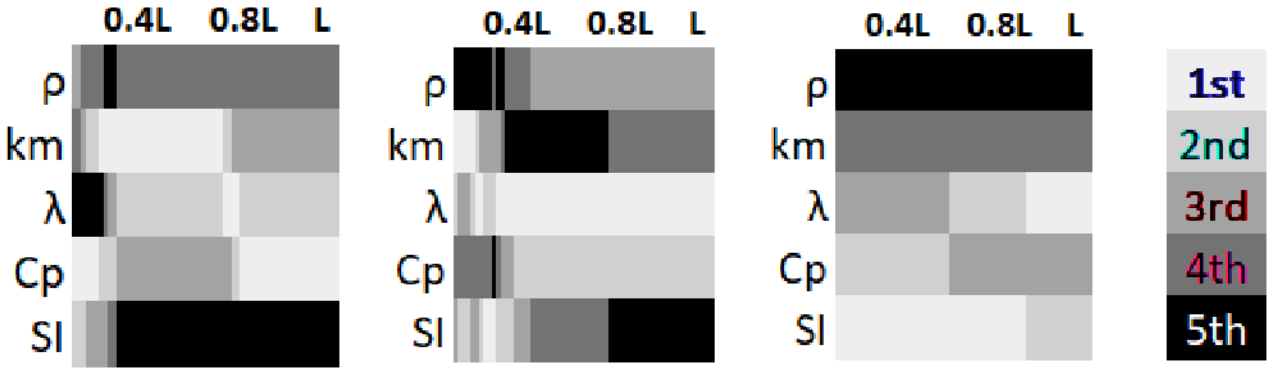

(a) Day 600 (summer) (b) Day 680 (autumn) (c) Day 760 (winter)

Fig. 10 Ranking of the influence of material properties through the wall depth for T output

around the null value, with a very low amplitude (usually lower than 100 Pa).

3.3 Relationship between material properties and model outputs

In accordance with the input meshing step, the Morris method makes possible to understand the relation between outputs and inputs through the σ/μ^* ratios. Figure 12 displays the evolution of σ/μ^* of the inputs for T and P_v outputs, at the mid-depth of the wall. A first overview led to the initial observation that there is a monotonic relationship between the material properties and the outputs as more than 90% of the σ/μ^*-ratio values were between 0.1 and 0.5, for both outputs (Section 2.3.1). A nearly constant ratio of 0.1−0.3 for T output was found for all inputs and of 0.2−0.3 for P_v output, for all inputs except *SI*. Indeed, the latter showed a quite linear relationship with P_v as σ/μ^* ratio oscillate around 0.1. As a matter of fact on P_v output, a seasonal effect was highlighted and related to the property. For instance, non-linear effects were mostly found during summer and spring seasons for C_p. For Hemp concrete, Benkhaled et al has found a monotonic quadratic relationship of λ and C_p with T output, *SI* and k_m with P_v output, using a LA method [61]. SI showed quite linear relationship with P_v output at high temperature gradients (summers) and the same level of monotony as other inputs during winter.

σ/μ^* ratio as well as its seasonal influence did not changed whatever the position trough the wall depth. The determinant parameter is the time necessary to reach steady state inside the wall (Fig. 17).

Table 3 ranks the noise of inputs on each output from the highest to the lowest one, according to the θ_i indicator. The noise produced by a property indicates the relationship's

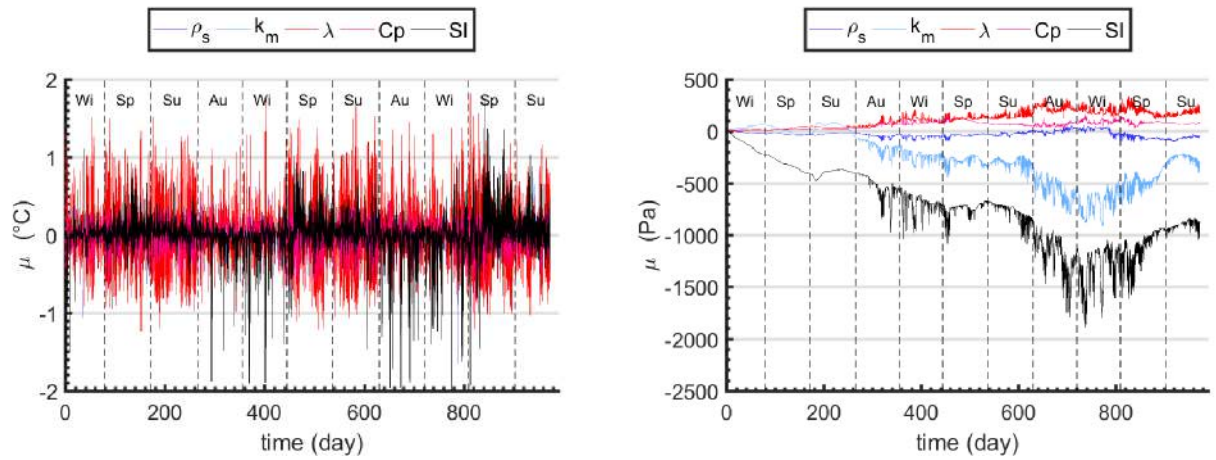

(a) on T output (b) on P_v output

Fig. 11 Evolution of μ indices of inputs with respect to time at 150 mm position (mid-depth)

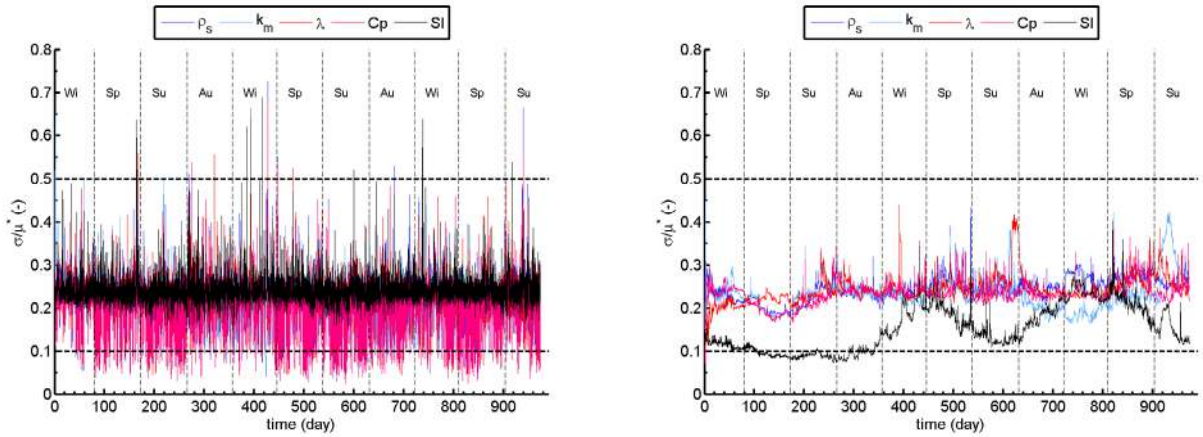

(a) on T output

(b) on P_v output

Fig. 12 σ/μ^*-ratio of the inputs at the wall mid-depth. Black-dashed horizontal lower and upper lines indicates $\sigma/\mu^* = 0.1$ and $\sigma/\mu^* = 0.5$, respectively, as defined in Section 2.3.1

Table 3 θ_i ratio at the mid-depth of the wall. The 95th percentile represents the value, for which 95% of the ratios are lower, during the 2.5 years time modelling. The higher is θ_i, the noisier is the property with respect to the considered output

	Temperature output				Vapor pressure output			
Input	5th perc	95th perc	θ_i	rank	5th perc	95th perc	θ_i	rank
ρ	0.13	0.34	0.22	3	0.20	0.36	0.16	2
k_m	0.20	0.35	0.16	5	0.17	0.30	0.13	4
λ	0.05	0.29	0.25	1	0.23	0.36	0.13	3
C_p	0.12	0.34	0.23	2	0.20	0.45	0.25	1
SI	0.18	0.34	0.16	4	0.09	0.18	0.09	5

level with the output. As a reminder, the higher θ_i is, the noisier the input is and hence, there is a high probability that material property i interacts with others properties. The ranking is almost identical for both seasons and thickness inside the wall, except at the start of transfers. On the temperature output, a quite steady inputs θ's (the same noisy level) was calculated for properties (0.025–0.16) unlike the vapour pressure output (0.09–0.25). For the latter, C_p was the noisiest property ($\theta_i = 0.25$), followed by ρ ($\theta_i = 0.16$). λ and k_m showed the same noise level ($\theta_i = 0.13$) and SI was the more stable property ($\theta_i = 0.09$). Indeed, the latter property showed a linear trend with P_v.

4 Conclusion

A sensitivity analysis of the influence of the cob material properties variability on a coupled thermal and moisture transfers model response through a cob wall has been conducted and showed that:

- the water vapour pressure (P_v) was very sensitive to the variation range of cob materials, unlike temperature (T). The static loading condition highlighted the large variability of P_v profiles during steady state, unlike the temperature profiles. Dynamic loading generates a continuous water vapour adsorption until an established dynamic transfers regime.
- The local analysis showed lower CVs of T and P_v profiles: for hygric properties variation on temperature output and for thermal properties on vapour pressure, unlike the global Analysis (Morris method). However a set of local analyses for all properties led to quite same results on P_v profiles as the Morris method. According to the μ_i^* Morris index, the effect on temperature profiles was globally negligible (up to 0.5 °C variation range by mean in all the cob depth), whereas great variation ranges on P_v profiles were found with sorption isotherm (up to 2000 Pa). Moreover, by using profiles through the wall depth, from high to low influential inputs, the following classification was identified: SI, k_m, λ, C_p and ρ.

- According to the μ-index, thermal properties showed positive correlation with P_v inside the material whereas hygric properties were negatively correlated with P_v output. Hence, the coupling of heat and moisture transfers is highlighted.
- According to the σ/μ^* index, the material properties showed a monotonic behaviour with the P_v outputs, except for the *SI* input. As a matter of fact, the latter input index was fairly changeable depending on the seasonal loading and the loading gradient. Thus, they were ranked according to the noise level provided. Thermal properties produced higher daily-noises. They were ranked as follows from the most to the least influential: C_p, ρ, λ, k_m and finally *SI*.

As a further work, a global sensitivity analysis based on the variance decomposition of the model's outputs variabilities could be conducted with quantitative indices to measure the relative contribution of inputs as well as their interactions. Moreover, this study could also be powered up by finding how the variability changes according to the boundary conditions, by finding the effect of lower thermo-diffusion transfers assumption, by including hysteresis of sorption isotherms and their temperature-dependency.

Appendix 1 Effect of the variability of properties on profiles

See Figs. 13, 14 and 15.

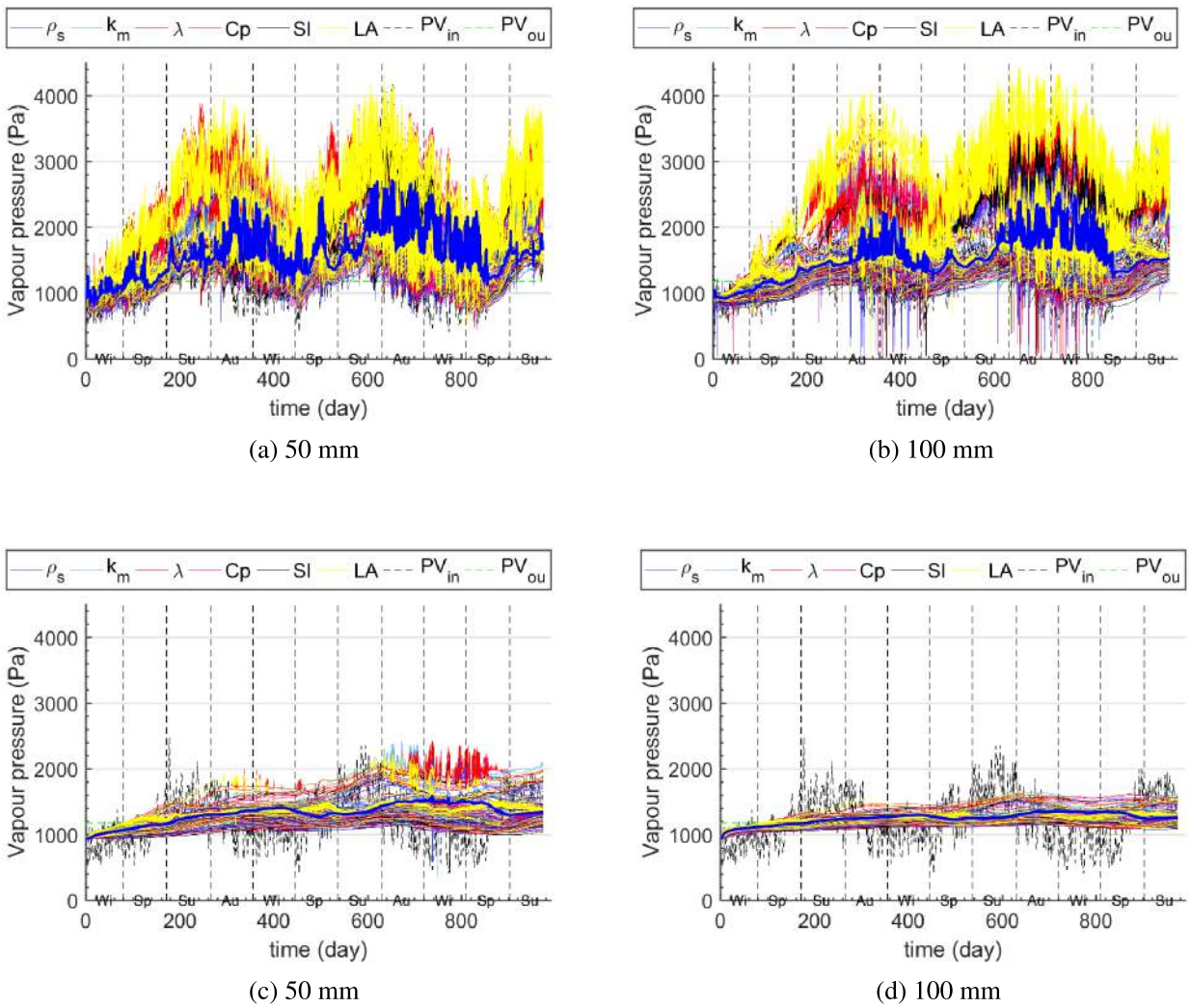

(a) 50 mm (b) 100 mm

(c) 50 mm (d) 100 mm

Fig. 13 Variability of P_v profiles

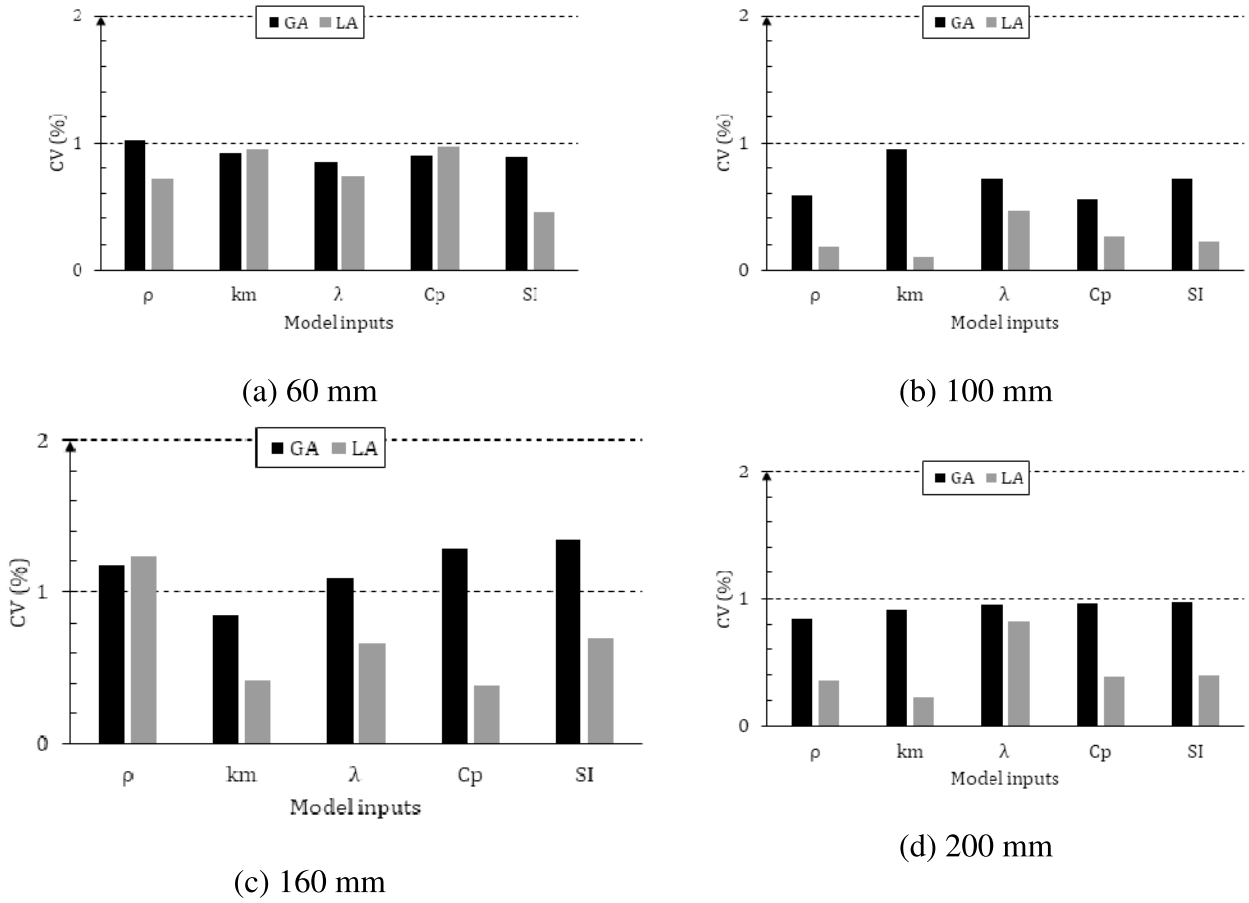

Fig. 14 CV of T profiles at wall mid-depth, for various seasons

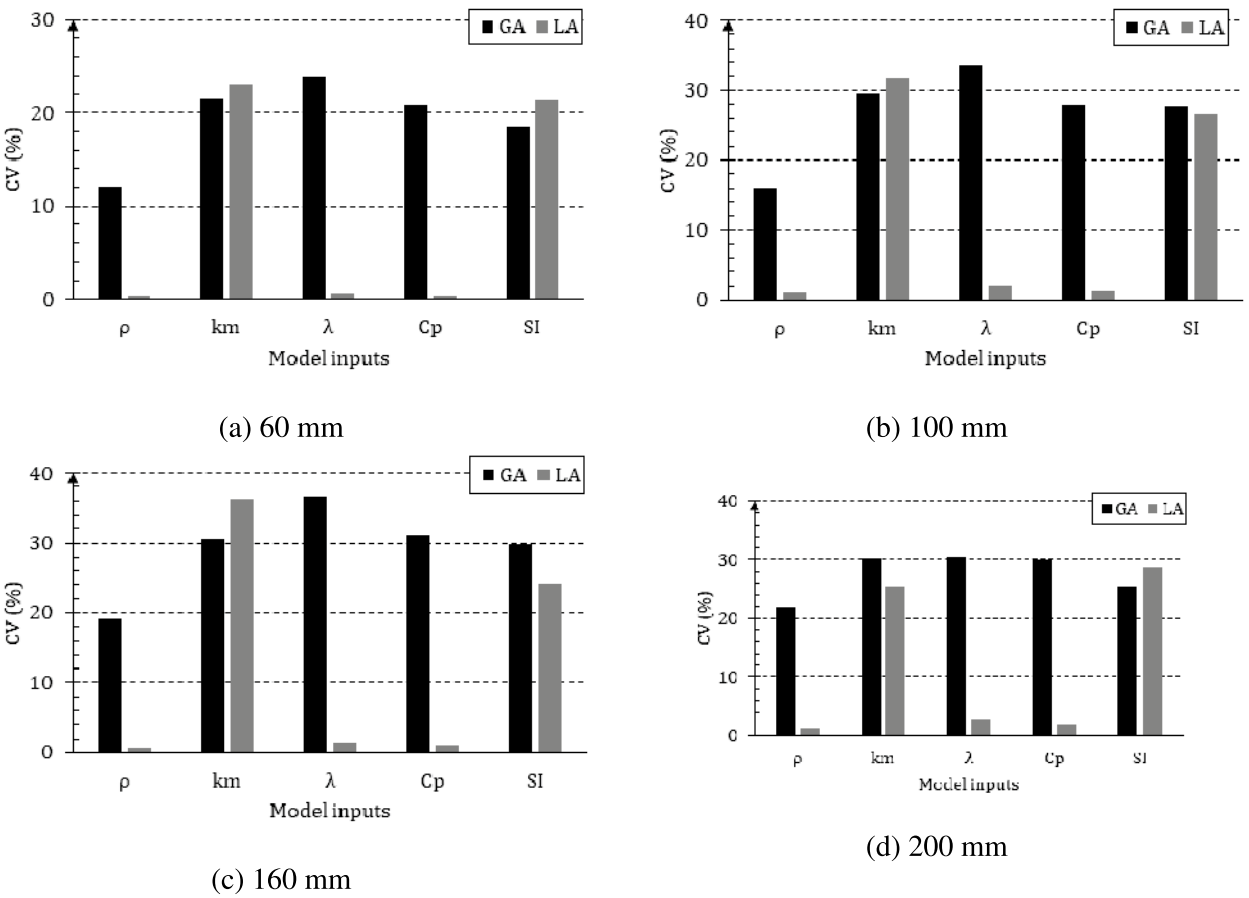

Fig. 15 CV of P_v profiles at wall mid-depth, for various seasons

Appendix 2 μ-indexes

See Figs. 16.

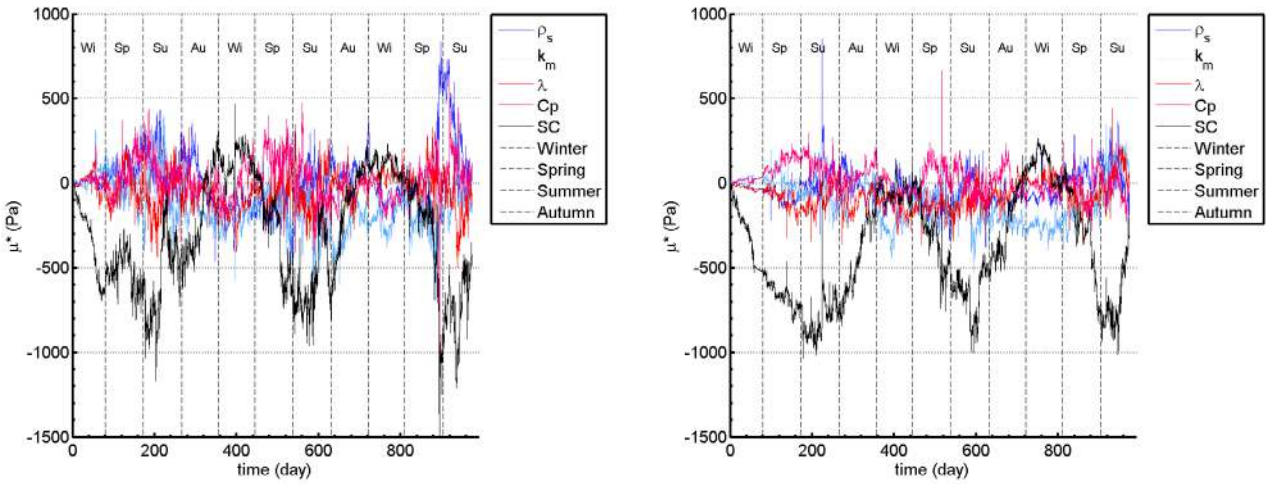

(a) 60 mm

(b) 100 mm

Fig. 16 μ-indices of P_v profiles

Appendix 3 σ/μ-indices

See Fig. 17.

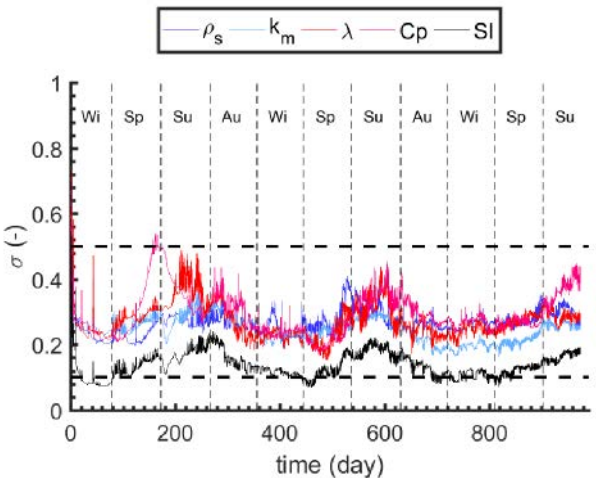

(a) 100 mm depth

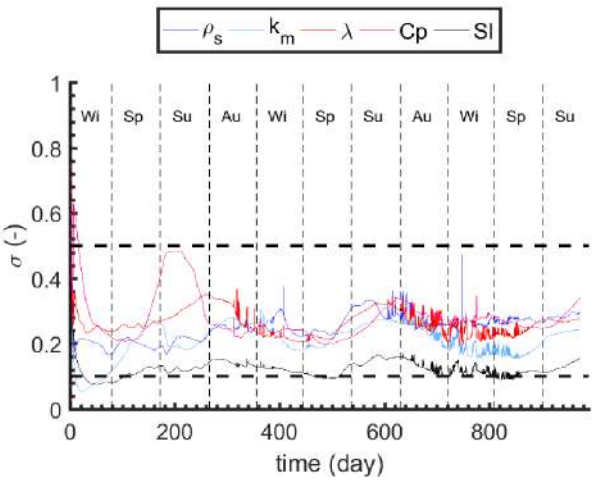

(b) 200 mm depth

Fig. 17 σ/μ^*-indices of P_v profiles

Author contributions the authors have participated equally in all stages of production of this material.

Funding The authors thank the Ecologic Transistion Agency (ADEME, France), the Pays de la Loire Region (France) and Palladio Foundation for supporting this work.

Data availability All data related to this paper are available under request.

Declarations

Conflict of interest On behalf of all authors, the corresponding author states that there is no conflict of interest.

References

1. Agence de la Transition écologique (ADEME), Chiffres clés du bâtiment, 2013
2. Roberts S (2008) Altering existing buildings in the UK. Energy policy 36(12):4482–4486
3. Wakili KG, Binder B, Zimmermann M, Tanner C (2014) Efficiency verification of a combination of high performance and conventional insulation layers in retrofitting a 130-year old building. Energy Build 82:237–242
4. Charai M, Mezrhab A, Moga L (2022) A structural wall incorporating biosourced earth for summer thermal comfort improvement: hygrothermal characterization and building simulation using calibrated PMV-PPD model. Build Environ 212:108842
5. Fabbri A, Morel JC, Aubert JE, Bui QB, Gallipoli D, Ventura A, Reddy VBV, Hamard E, Pelé-Peltier A, Abhilash HN (2022) An overview of the remaining challenges of the RILEM TC 274-TCE, testing and characterisation of earth-based building materials and elements. vol 6. pp 150–157
6. Künzel HM, Holm A, Zirkelbach D, Karagiozis AN (2005) Simulation of indoor temperature and humidity conditions including hygrothermal interactions with the building envelope. Sol Energy 78:554–561
7. Ferroukhi MY, Abahri K, Belarbi R, Limam K, Nouviaire A (2016) Experimental validation of coupled heat, air and moisture transfer modeling in multilayer building components. Heat Mass Transf 52:2257–2269
8. Philip JR, De Vries DA (1957) Moisture movement in porous materials under temperature gradients. Trans Am Geophys Union 38(2):222
9. Luikov AV (1975) Systems of differential equations of heat and mass transfer in capillary-porous bodies (review). Int J Heat Mass Transf 18:1–14
10. Moyne C (1987) Transferts couples chaleur-masse lors du séchage : prise en compte du mouvement de la phase gazeuse. PhD thesis, Vandoeuvre-les-Nancy, INPL
11. Hamard E (2017) Rediscovering of vernacular adaptative construction strategies for sustainable modern building: application to cob and rammed earth. PhD thesis, Université de Lyon
12. Vinceslas T (2019) Caractérisation d'éco-matériaux terre-chanvre en prenant en compte la variabilité des ressources disponibles localement. PhD thesis, Lorient
13. Aubert J-E (2013) Caractérisation des briques de terre crue de Midi-Pyrénées, tech. rep., Laboratoire de Recherche en Architecture (LRA) - ENSA Toulouse
14. Niroumand H, Zain MFM, Jamil M (2013) Various types of earth buildings. Procedia - Social and Behavioral Sciences 89:226–230
15. Hugo H, Guillaud H, CRAterre (2006) Traité de construction en terre. Editions Paranthèses
16. Ma C, Xie Y, Long G, Chen B, Chen L (2017) Effects of fly ash on mechanical and physical properties of earth-based construction. Constr Build Mater 157:1074–1083
17. Narayanaswamy AH, Walker P, Venkatarama Reddy BV, Heath A, Maskell D (2020) Mechanical and thermal properties, and comparative life-cycle impacts, of stabilised earth building products. Constr Build Mater 243:118096
18. Barbero-Barrera MM, Jové-Sandoval F, González Iglesias S (2020) Assessment of the effect of natural hydraulic lime on the stabilisation of compressed earth blocks. Constr Build Mater 260:119877
19. Toufigh V, Kianfar E (2019) The effects of stabilizers on the thermal and the mechanical properties of rammed earth at various humidities and their environmental impacts. Constr Build Mater 200:616–629

20. Imanzadeh S, Hibouche A, Jarno A, Taibi S (2018) Formulating and optimizing the compressive strength of a raw earth concrete by mixture design. Constr Build Mater 163:149–159
21. Perrot A, Rangeard D, Menasria F, Guihéneuf S (2018) Strategies for optimizing the mechanical strengths of raw earth-based mortars. Constr Build Mater 167:496–504
22. Laborel-Préneron A, Magniont C, Aubert J-E (2018) Hygrothermal properties of unfired earth bricks: effect of barley straw, hemp shiv and corn cob addition. Energy Build 178:265–278
23. Laborel-Préneron A, Aubert JE, Magniont C, Tribout C, Bertron A (2016) Plant aggregates and fibers in earth construction materials: a review. Constr Build Mater 111:719–734
24. Ashour T, Wieland H, Georg H, Bockisch F-J, Wu W (2010) The influence of natural reinforcement fibres on insulation values of earth plaster for straw bale buildings. Mater Des 31:4676–4685
25. Hall M, Allinson D (2009) Assessing the effects of soil grading on the moisture content-dependent thermal conductivity of stabilised rammed earth materials. Appl Therm Eng 29:740–747
26. Cagnon H, Aubert JE, Coutand M, Magniont C (2014) Hygrothermal properties of earth bricks. Energy Build 80:208–217
27. Baescher GB, Christian JT (2008) Spatial variability and geotechnical reliability. In: Reliability-Based Design in Geotechnical Engineering: Computations and Applications. pp 76–133
28. Iooss B, Lemaître P (2015) A review on global sensitivity analysis methods. In: Meloni C, Dellino G (eds) Uncertainty management in Simulation-Optimization of Complex Systems: Algorithms and Applications. Springer
29. Hawila AAW, Merabtine A (2021) A statistical-based optimization method to integrate thermal comfort in the design of low energy consumption building. J Build Eng 33:101661
30. Andrianandraina Ventura A, Kiessé TS, Cazacliu B, Idir R, Werf HMGVD (2015) Sensitivity analysis of environmental process modeling in a life cycle context: a case study of hemp crop production. J Ind Ecol 19(6):978–993
31. Goffart J, Woloszyn M (2018) RBD-FAST: une méthode d'analyse de sensibilité rapide et rigoureuse pour la garantie de performance énergétique, Conférence IBPSA France - Bordeaux. p 9
32. Stéphan E, Caucheteux A, Cantin R, Tasca-Guernouti S, Michel P (2013) Sensitivity analysis of an energyplus simulation model of the ambient humidity in an old building. In: 13th Conference of International Building Performance Simulation. Chambéry, France
33. Delgarm N, Sajadi B, Azarbad K, Delgarm S (2018) Sensitivity analysis of building energy performance: a simulation-based approach using OFAT and variance-based sensitivity analysis methods. J Build Eng 15:181–193
34. Senga Kiessé T, Ventura A, van der Werf HMG, Cazacliu B, Idir R, Andrianandraina (2017) Introducing economic actors and their possibilities for action in LCA using sensitivity analysis: application to hemp-based insulation products for building applications. J Clean Prod 142:3905–3916
35. Van-Loc TA, Senga Kiesse T, Bonnet S, Ventura A (2018) Application of sensitivity analysis in the life cycle design for the durability of reinforced concrete structures in the case of XC4 exposure class. Cem Concr Compos 87:53–62
36. Senga Kiesse T, Bonnet S, Amiri O, Ventura A (2020) Analysis of corrosion risk due to chloride diffusion for concrete structures in marine environment. Mar Struct 73:102804
37. Othmen I, Poullain P, Leklou A-N, Caucheteux A (2014) Sensitivity analysis of the Künzel model: application to the study of the hygrothermal transfer in a tuffeau wall. In: Heat Transfer XIII:Simulation and Experiments in Heat and Mass Transfer, WIT Press
38. Le Tran AD, Maalouf C, Mai TH, Wurtz E, Collet F (2010) Transient hygrothermal behaviour of a hemp concrete building envelope. Energy Build 42:1797–1806
39. Bui R, Goffart J, McGregor F, Woloszyn M, Fabbri A, Grillet A-C (2020) Uncertainty and sensitivity analysis applied to a rammed earth wall: evaluation of the discrepancies between experimental and numerical data. In: E3S Web of Conferences, vol 172. p 17004
40. Issaadi N (2015) Effets de la variabilité des propriétés de matériaux cimentaires sur les transferts hygrothermiques : développement d'une approche probabiliste. PhD thesis, Université La Rochelle, Ecole royale militaire de Bruxelles
41. Morris MD (1991) Factorial sampling plans for preliminary computational experiments. Technometrics 33(2):161–174
42. Qin M, Belarbi R, Aît-Mokhtar A, Nilsson L-O (2008) Simultaneous heat and moisture transport in porous building materials transport properties: evaluation of nonisothermal moisture. J Mater Sci 43:3655–3663
43. Abahri K, Belarbi R, Trabelsi A (2011) Contribution to analytical and numerical study of combined heat and moisture transfer in porous building materials. Build Environ 46:1354–1360
44. Allam R, Nabil I, Belarbi R, El-Meligy M, Altahrany A (2018) Hygrothermal behavior for a clay brick wall. vol 54
45. Gandia RM, Gomes FC, Corrêa AAR, Rodrigues MC, Mendes RF (2019) Physical, mechanical and thermal behavior of adobe stabilized with glass fiber reinforced polymer waste. Constr Build Mater 222:168–182
46. Labat M, Magniont C, Oudhof N, Aubert J-E (2016) From the experimental characterization of the hygrothermal properties of straw-clay mixtures to the numerical assessment of their buffering potential. Build Environ 97:69–81
47. El Fgaier F, Lafhaj Z, Brachelet F, Antczak E, Chapiseau C (2015) Thermal performance of unfired clay bricks used in construction in the north of France: case study. Case Stud Constr Mater 3:102–111
48. Maillard P, Aubert JE (2014) Effects of the anisotropy of extruded earth bricks on their hygrothermal properties. Constr Build Mater 63:56–61
49. Barnaure M, Stéphanie B, Poullain P (2021) Earth buildings with local materials: assessing the variability of properties measured using non-destructive methods. Constr Build Mater
50. Medjelekh D, Ulmet L, Dubois F (2017) Characterization of hygrothermal transfers in the unfired earth. Energy Procedia 139:487–492
51. Janssen H (2019) A discussion of "Analysis of the water absorption test to assess the intrinsic permeability of earthen materials." Constr Build Mater 215:1044–1046
52. Fabbri A, Soudani L, McGregor F, Morel J-C (2019) Closure to the discussion of "Analysis of the water absorption test to assess the intrinsic permeability of earthen materials." Constr Build Mater 216:362–364
53. Fabbri A, Soudani L, McGregor F, Morel J-C (2019) Analysis of the water absorption test to assess the intrinsic permeability of earthen materials. Constr Build Mater 199:154–162
54. Castagnède B, Aknine A, Brouard B, Tarnow V (2000) Effects of compression on the sound absorption of fibrous materials. Appl Acoust 61:173–182
55. Ben Mansour M, Ogam E, Jelidi A, Cherif AS, Ben Jabrallah S (2017) Influence of compaction pressure on the mechanical and acoustic properties of compacted earth blocks: an inverse multiparameter acoustic problem. Appl Acoust 125:128–135
56. Tchiotsop J (2023) Experimental and numerical studies of the variability of hygrothermal properties effects on the coupled heat and moisture transfer through a cob wall: material and wall scales. PhD thesis, Nantes Université. unpublished thesis
57. Laborel-Préneron A, Magniont C, Aubert J-E (2018) Hygrothermal properties of unfired earth bricks: effect of barley straw, hemp shiv and corn cob addition. Energy Build 178:265–278
58. Timmermann EO (2003) Multilayer sorption parameters: BET or GAB values? Colloids Surf A Physicochem Eng Asp 220:235–260
59. Goffart J (2013) Impact of the variability of weather data on a low energy house. Application of Sensitivity Analysis for Correlated Temporal Inputs

60. May Tzuc O, Rodríguez Gamboa O, Aguilar Rosel R, Che Poot M, Edelman H, Jiménez Torres M, Bassam A (2021) Modeling of hygrothermal behavior for green facade's concrete wall exposed to nordic climate using artificial intelligence and global sensitivity analysis. J Build Eng 33:101625
61. Benkhaled M, Ouldboukhitine S-E, Bakkour A, Amziane S (2022) Sensitivity analysis of the parameters for assessing a hygrothermal transfer model HAM in bio-based hemp concrete material. International Communications in Heat and Mass Transfer 132:105884